THE EUROPEAN
PHYSICAL JOURNAL PLUS

Neutron capture reaction cross section measurement for iodine nucleus with detailed uncertainty quantification

A. Gandhi[1,a]**, Aman Sharma**[1]**, Rebecca Pachuau**[1]**, Namrata Singh**[1]**,**
Prashant N. Patil[2]**, Mayur Mehta**[3]**, L. S. Danu**[4]**, S. V. Suryanarayana**[4]**, B. K. Nayak**[4]**,**
B. Lalremruata[5]**, A. Kumar**[1,b] (ID)

[1] Department of Physics, Banaras Hindu University, Varanasi 221005, India
[2] Department of Studies in Physics, Karnatak University, Dharwad 580003, India
[3] Institute for Plasma Research, Gandhinagar 382428, India
[4] Nuclear Physics Division, Bhabha Atomic Research Centre, Mumbai 400085, India
[5] Department of Physics, Mizoram University, Aizawl, Tanhril 796004, India

Abstract The neutron activation cross section for ^{127}I(n,γ)^{128}I reaction has been experimentally measured with respect to the ^{115}In(n,inl)^{115}In^m reference monitor reaction cross section in the neutron spectrum average energy range $0.60--2.51$ MeV. The neutrons were produced through ^{7}Li(p,n)^{7}Be reaction, and γ-ray spectra of the residue product were measured offline with the precalibrated lead-shielded HPGe detector. The very first time the covariance analysis was done to quantify the measured cross section uncertainties and the correlation coefficients between the different neutron energy cross sections for iodine nucleus. The needful corrections related to the γ-ray self-attenuation process, γ-ray true coincidence summing effect and the low background neutron energy contributions were considered in the present measurement. Theoretical calculations were done using the standard nuclear reaction model codes TALYS-1.9 and EMPIRE-3.2 to obtain the ^{127}I(n,γ)^{128}I reaction cross section. The measured cross sections were compared with the experimental data available in the EXFOR database, theoretical predicted results, and ENDF/B-VIII.0, JEFF-3.1/A, TENDL-2019, and JENDL-4.0 evaluated nuclear data.

1 Introduction

The neutron capture cross section is important for the studies of nuclear physics phenomena like nuclear reaction dynamics, element formation, and the nucleosynthesis process in astrophysics. Its quantitative values are essential for the safety analysis and design of reactors [1,2]. In the low-energy neutron region, the quantitative value of (n,γ) reaction cross section of iodine nucleus is also considered as a standard monitor in the neutron activation experiments [3]. The experimental capture cross sections are also essential to test the sensitivity and validation of different parameters used by the statistical model codes [4]. The KI (potas-

[a] e-mail: gandhiaman653@gmail.com
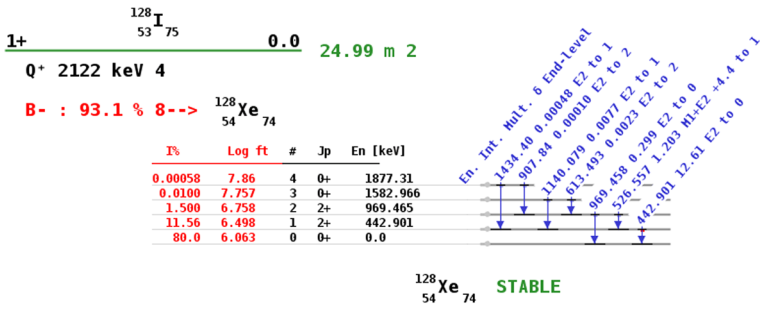
[b] e-mail: ajaytyagi@bhu.ac.in (corresponding author)

Fig. 1 Decay scheme of the ^{128}I existed nucleus

sium iodide), a salt of stable iodine nucleus, also helps to block the radioactive iodine from being absorbed by the thyroid gland, thus protecting this gland from radiation injury [5]. ^{127}I is the only natural exiting iodine isotope that forms the ^{128}I excited compound nucleus on neutron capture and it β-decays to stable nucleus ^{128}Xe with a half-life ($t_{1/2} = 24.99 \pm 0.02$ min). This β-decay process produces the high-intense γ-ray of energy 442.90 keV with a 12.61% gamma intensity, which is used in the present case for determining the (n,γ) cross section. The decay scheme of ^{128}I nucleus is shown in Fig. 1 retrieved from the NNDC [6]. Considering the requirements mentioned above, we have planned to carry out the neutron capture cross section measurement for the iodine nucleus with more accuracy and detailed uncertainty quantification. In the present work, the (n,γ) reaction cross section for ^{127}I target nucleus was measured with respect to the ^{115}In(n,inl)^{115}In^m reference monitor reaction cross section in the neutron spectrum average energy range, $0.60--2.51$ MeV. In this manuscript, the experimentally measured cross sections are provided with a detailed description of the uncertainty measurement, which were missing in the literature. This detailed description of the uncertainty is essential information required in evaluation of nuclear data, which is used by the users to check the performance and safety metrics for a given application [7–10]. The obtained results are compared with the previously measured data retrieved from the IAEA-EXFOR database [11,12], and ENDF/B-VIII.0, JEFF-3.1/A, TENDL-2019, and JENDL-4.0 evaluated nuclear data [13–16]. The cross section was also computed theoretically using the statistical model codes TALYS-1.9 and EMPIRE-3.2. The calculated theoretical results by TALYS-1.9 and EMPIRE-3.2 were compared with the present measured cross section, existing, and the evaluated data.

Section 2 describes the experimental details and the methodology used for measuring the cross section, while Sect. 3 provides the detail about the nuclear model calculations. Section 4 contains the results and discussion part.

2 Experimental details and methodology

The experimental measurement of the ^{127}I(n,γ)^{128}I reaction cross section was carried out with the neutrons based on the $p+^7$Li$\longrightarrow n+^7$Be reaction (Q value $= -1.644$ MeV; $E_{th} = 1.880$ MeV) [17,18]. The FOTIA (charged-particle accelerator) facility at Bhabha Atomic Research center (BARC), Mumbai, was used for the proton beam production [19]. The proton beam current during the experiment was 100 nA, and the proton beam of energies E$_p$ = 2.6, 3.2 and 4.4 MeV were shot on a natural ^{7}Li metallic target. The proton energy spread was 0.02 MeV produced from the accelerator. The ^{7}Li-target was stuck at the back side of the
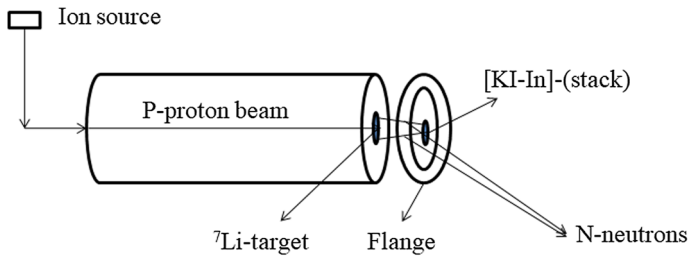
Fig. 2 ^{7}Li$(p,n)^7$Be reaction-based neutrons irradiation set-up

flange, and the target stack to be irradiated was pasted at the front side of the flange. The neutron irradiation set-up is presented in Fig. 2, and the quantitative details related to the irradiation are given in Table 1.

For the present measurement, a highly pure KI (potassium iodide) powder was used in the shape of a pellet with a diameter of 1 cm and a thickness of 0.3 cm packed in a polythene bag. The natural indium foil with a thickness of 0.05 cm enfold in a pure aluminium foil of thickness 0.025 mm was used for the neutron monitor. ^{115}In$(n,inl)^{115}$In^m reaction was considered as a reference reaction for the monitor. IRDFF-1.05 standard data library was used to get the cross section of monitor reaction [20]. In the experimental set-up, the activation sample was placed at a distance of 9.0 mm from the ^{7}Li-target, and the stack of activation samples was placed at zero degrees with respect to the beam direction. The other details of the activation samples are summarized in Table 2.

Since in the present experiment we have used the continuous proton beam produced from the FOTIA accelerator, hence, the time-of-flight technique cannot be implemented to get the spectrum of neutron energy, and therefore, the simulation code EPEN-(Energy of Proton Energy of Neutron) was used [21,22]. EPEN is a specially designed simulation code based on the ^{7}Li$(p,n)^7$Be reaction for the evaluation of neutron flux energy spectrum. The code works for the incident proton energies from the reaction threshold (i.e. 1.880 MeV) to 7.0 MeV. The detail about the input parameters and formalism used in the EPEN code to produce the neutron flux energy spectrum has been provided in Ref. [21]. The present incident proton energies exceed the energy threshold of the 1st excited energy level of ^{7}Be (i.e. 2.37 MeV) and threshold (i.e. 3.70 MeV) of three-body breakup ^{7}Li$(p,n+^3He)^4$He reaction; therefore, the neutrons of interest are accompanied by the lower energy background neutrons produced through ^{7}Li$(p,n_1)^7$Be* reaction and also the neutron yield from ^{7}Li$(p,n+^3He)^4$He reaction channel. The magnitude of the neutron production yield from ^{7}Li$(p,n+^3He)^4$He reaction channel is negligible at the present proton energy, whereas the magnitude of (p,n_0) group neutron yield is around 90% followed by the magnitude from ^{7}Li$(p,n_1)^7$Be*, which is less than 10% [23,24]. To account for the correction of the contribution or the magnitude of the lower energy neutron from ^{7}Li$(p,n_1)^7$Be* reaction, the needful correction has been done in the present work and is discussed in subsection 2.2. The neutron flux energy spectrum of (p,n_0) and (p,n_1) group neutrons obtained from EPEN code is presented in Figs. 3–4. It can be observed that the neutron spectrums of (p,n_0) are having a spread which is due to the proton energy loss in the ^{7}Li target and the neutron spectrum average energy value produced from ^{7}Li$(p,n_0)^7$Be reaction was obtained by using the following equation given by [25,26]

$$< E_n >= [\frac{\int E \times \Phi_0(E)dE}{\int \Phi_0(E)dE}] \tag{1}$$

Table 1 Details of the neutron irradiations of the present measurement

E_p (MeV)	Beam current (nA)	$< E_n >$ (MeV)	Neutron flux $(n/cm^2/s^1) \times 10^6$
2.6	100	0.60	5.406
3.2	100	1.26	2.202
4.4	100	2.51	3.456

where the neutron flux for (p,n_0) energy spectrum is denoted by $\Phi_0(E)$ obtained from EPEN code. For E_p = 2.6, 3.2, and 4.4 MeV, the spectrum-averaged neutron energies with their energy spread estimated using EPEN code are 0.60 ± 0.01 MeV, 1.26 ± 0.02 MeV, and 2.51 ± 0.02 MeV, respectively.

2.1 Offline γ-ray spectroscopy

The activation samples were irradiated with the neutrons up to the fifth half-life of residue product (^{128}I) to produce enough induced activity in the samples. After the exposure of neutrons in the targets, the irradiated targets were brought from the experimental hall to the gamma counting room for the offline γ-ray spectroscopy. The induced activity in the iodine sample was counted after the cooling interval, and then, the induced activity in the indium foil was counted. The timing details of the present measurement, such as irradiation (t_{irr}), cooling (t_{cool}), and counting (t_{count}) times, are summarized in Table 3, and the decay data details of the sample and monitor reactions are summarized in Table 4. The induced activity of 442.90 and 336.24 keV high-intense γ-rays produced from ^{127}I$(n,\gamma)^{128}$I and ^{115}In$(n,inl)^{115}$In^m reactions, respectively, were measured with the precalibrated 185-cc HPGe detector system whose relative efficiency was 30% and the energy resolution was 1.8 keV for 1.33 MeV γ-ray energy of ^{60}Co. The CAMAC-based LAMPS software was used for the data acquisition and analysis. The calibration and efficiency measurement of the detector were done with the ^{152}Eu point-source, having initial activity (A_0) = 6659.21 $\pm$ 81.60 Bq as on 01-10-1999 with a half-life ($t_{1/2}$ = 13.517 $\pm$ 0.009 y [29]). The detector efficiency for the point source is calculated using the following equation:

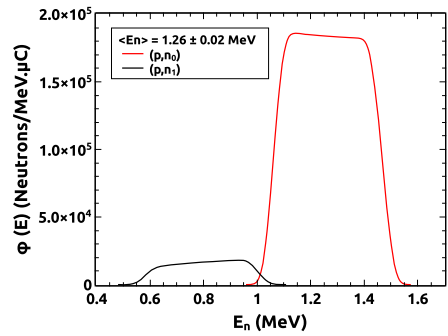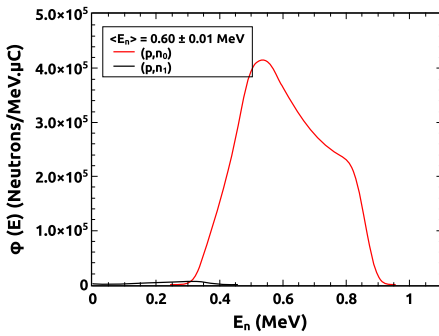$$\varepsilon_p = \left[\frac{C K_c}{A_0 I_\gamma e^{-\lambda t} \Delta t} \right] \tag{2}$$

where C is the photo-peak counts for a particular γ-ray energy (E_γ) in the counting time ($\Delta t = 4800$ s), and I_γ is the gamma intensity for a particular E_γ of ^{152}Eu point-source retrieved from ENSDF [29]. K_c is the correction factor for γ-ray coincidence summing effect calculated using the EFFTRAN code [30,31], and t is the elapsed time between the date of manufacture of the source and the date of counting. The distance between the target/source and the detector endcap was 2.0 mm. The obtained efficiency value for the point source (ε_p) was transferred to the efficiency for the sample geometry source (ε) using the EFFTRAN code, which are summarized in Table 5. The efficiency value of the characteristic γ-ray energy is calculated using the following equation

$$\varepsilon(E_\gamma) = \left[\varepsilon_o exp(-E_\gamma/E_0) + \varepsilon_c \right] \tag{3}$$

where (ε_c, ε_o, and E_0) are the fitting parameters of the above-mentioned function [25,32]. The interpolated efficiency fitting curve along with the efficiency data points (ε) is plotted in

Table 2 Activation samples' details of the present measurement

$< E_n >$ (MeV)	Isotope	Irradiated Sample	Isotope Abundance (%)	Thickness (cm)	Density (g/cm^3)	Isotope weight in The sample (mg)	Number of target atoms (10^{-4} atoms/b)
0.60	^{127}I	KI powder	100	0.3	3.13	431.7 ± 0.1	20.48
1.26						374.1 ± 0.1	17.75
2.51						404.4 ± 0.1	19.18
0.60	^{115}In	In foil	95.71 ± 0.05	0.05	7.31	185.2 ± 0.1	09.70
1.26						177.5 ± 0.1	09.30
2.51						191.4 ± 0.1	10.03

Fig. 3 Neutron spectrum generated from EPEN code for E_p = 2.6 ± 0.02 MeV (left) and E_p = 3.2 ± 0.02 MeV (right)

Fig. 4 Neutron spectrum generated from EPEN code for E_p = 4.4 ± 0.02 MeV
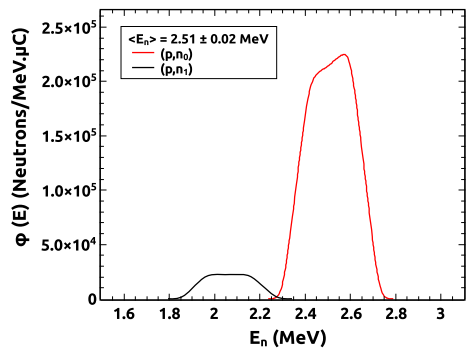
Table 3 Timing details of the present measurement

< E_n > (MeV)	Reaction	t_{irr} (s)	t_{cool} (s)	t_{count} (s)
0.60		6840	194	614
1.26	$^{127}I(n,\gamma)^{128}I$	7320	163	602
2.51		7975	365	1080
0.60		6840	832	721
1.26	$^{115}In(n,inl)^{115}In^m$	7320	4031	660
2.51		7975	3317	601

Table 4 Decay data parameters and their uncertainties considered in the present data analysis

Reaction	Residue product	Half-life ($t_{1/2}$)	E_γ (keV)	I_γ (%)	Reference
$^{127}I(n,\gamma)$	^{128}I	24.99 ± 0.02 min	442.90	12.61 ± 0.08	[27]
$^{115}In(n,inl)$	$^{115}In^m$	4.486 ± 0.004 h	336.24	45.9 ± 0.1	[28]

Table 5 Detailed data set of the different attributes involved in the detector calibration and analysis of the efficiency measurement of the HPGe detector

E_γ (keV)	I_γ	Counts (C)	K_c	ε_p	ε
121.78	0.2853 ± 0.0016	325692.0 ± 7723.8	1.165	0.052143	0.051778 ± 0.001413
244.69	0.0755 ± 0.0004	57207.9 ± 940.3	1.230	0.036540	0.036285 ± 0.000769
344.27	0.2659 ± 0.0020	167719.9 ± 2992.7	1.113	0.027525	0.027332 ± 0.000626
411.11	0.02238 ± 0.00013	9837.2 ± 252.5	1.288	0.022206	0.022051 ± 0.000640
778.90	0.1293 ± 0.0008	35816.8 ± 498.8	1.165	0.012652	0.012564 ± 0.000246
867.38	0.0423 ± 0.0003	9139.4 ± 164.0	1.274	0.010792	0.010716 ± 0.000245
964.05	0.1451 ± 0.0007	35076.6 ± 546.6	1.099	0.010416	0.010343 ± 0.000211
1112.94	0.1367 ± 0.0008	30554 ± 795.1	1.045	0.009157	0.009093 ± 0.000267
1408.01	0.2087 ± 0.0009	37166 ± 775.1	1.069	0.007463	0.007411 ± 0.000182

Fig. 5. The value of linear correlation coefficient (R) of the data fitting in Fig. 5 is 0.99835. The obtained fitting parameters' value along with its covariance matrix is summarized in Table 6, which is further needed to generate the covariance matrix between the interpolated efficiencies of the characteristic γ-ray energy of the residue products [7,25]. The covariance matrix has been generated by using the methodology as given in equation 38 of Ref. [7]. The obtained results of interpolated detector efficiency for the characteristic γ-ray energy of the sample (^{128}I, ε_s) and monitor (^{115}In^m, ε_m) residue products with its covariance matrix are summarized in Table 7. The above-given methodology for calculating the interpolated efficiencies and covariance matrix between them also has been used in our previous report [33,34].

2.2 Cross section determination and its uncertainty quantification

The cross section ($< \sigma_s >$) for ^{127}I$(n,\gamma)^{128}$I reaction was determined using the following neutron activation formula

$$< \sigma_s >=< \sigma_m > \times [\eta] \times \left[\frac{A_s I_m \lambda_s a_m N_m f_m}{A_m I_s \lambda_m a_s N_s f_s} \right] \times \left[\frac{C_{\gamma(s)} * N_{low(s)}}{C_{\gamma(m)} * N_{low(m)}} \right] \tag{4}$$

where ($< \sigma_m >$) is the monitor cross section averaged over the (p,n_0) neutron flux energy spectrum, ($A_{s,m}$) is the activity of γ-rays produced from the reaction residue detected by the HPGe detector, ($I_{s,m}$) is the γ-ray intensity of the characteristic γ-ray of the residue product, ($\lambda_{s,m}$) is the decay constant for the residue product, (η) is equal to the ratio of sample and monitor efficiency, ($a_{s,m}$) is the isotopic abundance, and ($N_{s,m}$) is the number of the target atoms. The timing factor for the sample and monitor reactions ($f_{s,m}$) is calculated by the following equation

$$f_{s,m} = \left[1 - e^{-\lambda t_{irr}} \right] \times e^{-\lambda t_{cool}} \times \left[1 - e^{-\lambda t_{count}} \right] \tag{5}$$

where the symbol t_{irr}, t_{cool}, and t_{count} are defined above in subsection 2.1. In the cross section calculations, we have also considered the corrections related to the γ-ray self-attenuation (C_γ) and low-energy background neutron contribution (N_{low}) correction factor in the cross section formula. The discussion of the correction factors due to C_γ and N_{low} is given below followed by the approach for calculating spectrum-averaged monitor cross sections, as well as their uncertainties and correlation coefficients.

Fig. 5 Interpolated detector efficiency fitting curve along with the measured detector efficiency (ε)
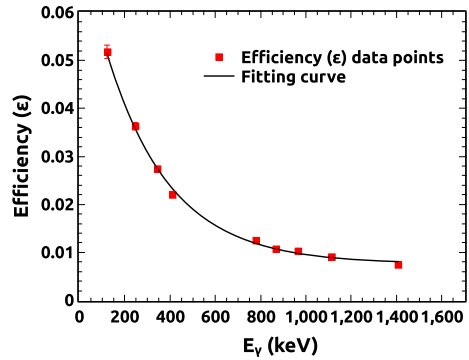
Table 6 Parameter values of the efficiency (ε) fitting curve with its covariance matrix

Parameters	Value	Covariance matrix		
ε_c	$0.00761 \pm 4.32300 \times 10^{-4}$	1.8688×10^{-7}		
ε_0	0.0675 ± 0.00278	5.24×10^{-7}	7.70×10^{-6}	
E_0 (keV)	281.36776 ± 15.5658	-0.0052	-0.03545	242.294

Table 7 Efficiency of the HPGe detector for the γ-rays produced from the residues of sample and monitor reactions with their uncertainty and covariance matrix

Reaction	E_γ (keV)	Efficiency	Covariance matrix	
^{127}I$(n,\gamma)^{128}$I	442.90	0.02151 ± 0.00050	2.5669×10^{-7}	
^{115}In$(n,inl)^{115}$In^m	336.24	0.02795 ± 0.00052	2.4921×10^{-7}	2.7151×10^{-7}

2.2.1 Correction factor (C_γ):

The correction factor (C_γ) for the self-absorption of γ-ray within the sample is determined using the equation [35–37]

$$C_\gamma = \left[\frac{\mu_m \rho d}{1 - exp(-\mu_m \rho d)} \right] \tag{6}$$

where the thickness of the sample is denoted by (d) having density (ρ), and the mass attenuation coefficient is represented by (μ_m). The XMuDat version 1.0.1 [38] software was used to calculate the mass attenuation coefficient for each sample. The obtained self-attenuation factor for a corresponding γ-ray energy of the residue product is given in Table 8.

2.2.2 Correction factor (N_{low}):

The incident proton energies in the present experiment are exceeding the energy threshold of the 1st excited level of ^{7}Be, and therefore, the neutrons produced from ^{7}Li$(p,n_0)^7$Be reaction contain contribution from the lower energy background neutrons produced by the ^{7}Li$(p,n_1)^7$Be* reaction. Since the (n,γ) reaction cross section is very sensitive with neutron energy, therefore, the subtraction of this (p,n_1) neutron background is extremely important for

Table 8 Correction factors (C_γ and N_{low}) considered in the measured (n,γ) cross section

Reaction	Sample	E_γ (keV)	C_γ	$< E_n >$ (MeV)	N_{low}
$^{127}I(n,\gamma)^{128}I$	KI	442.90	1.0707	0.60	0.9855
				1.26	0.8889
				2.51	0.8864
$^{115}In(n,inl)^{115}In^m$	In foil	336.24	1.0257	0.60	0.9993
				1.26	0.9749
				2.51	0.9194

the precise determination of (n,γ) cross section [22,25,39]; hence, this low energy correction has been considered and calculated by using the equation 13 of Ref. [25]

$$N_{low} = 1 - \left[\frac{\int \Phi_1(E)(\sigma_x(E))dE}{\int \Phi(E)(\sigma_x(E))dE} \right] \qquad (7)$$

where $\Phi_1(E)$ is the neutron flux for (p,n_1) energy spectrum, and $\Phi(E)$ is the total neutron energy flux $[\Phi_0(E) + \Phi_1(E)]$ obtained from the EPEN code. $\sigma_x(E)$ is the $^{127}I(n,\gamma)^{128}I$ reaction cross section retrieved from the ENDF/B-VIII.0 [13] and $^{115}In(n,inl)^{115}In^m$ reaction cross section retrieved from the IRDFF-1.05 data library [20]. Table 8 summarizes the correction factor (N_{low}) obtained for each neutron energy.

2.2.3 Neutron spectrum-averaged monitor cross section ($< \sigma_m >$):

In the present work, $^{115}In(n,inl)^{115}In^m$ reaction was taken as the reference monitor reaction and its cross section values were retrieved from the standard data library of the neutron monitor cross sections, IRDFF-1.05 [20]. In the defined incident proton energies, the production of neutrons from $^7Li(p,n)$ reaction is not monoenergetic but has some energy spread; therefore, the IRDFF-1.05 monitor cross section $[\sigma_m(E)]$ has been folded by the (p,n_0) neutron spectrum generated from the EPEN code [21,22] using the equation given by [25]

$$< \sigma_m > = \left[\frac{\int \Phi_0(E)\sigma_m(E)dE}{\int \Phi_0(E)dE} \right] \qquad (8)$$

We defined the group-wise neutron flux energy spectrum $\Phi_{i,j}$, generated from EPEN code by equation 9, as the same as a group-wise cross section with covariance information of $(\sigma_m(E))$ provided in the IRDFF-1.05 library to quantify the uncertainties and correlation coefficients between the different energies monitor cross sections for the current work

$$\Phi_{i,j} = \int_{Ej,min}^{Ej,max} \Phi_i(E)dE \qquad (9)$$

which satisfy the condition $\sum_j \Phi_{i,j} = 1$ and here i is specified as $= 1, 2,$ and 3 for averaged neutron energy $< E_n > = 0.60, 1.26,$ and 2.51 MeV. For each i, there are j energy groups defined by the energy group boundaries in IRDFF-1.05 library. The lower and upper boundaries of the jth energy group were defined by $E_{j,min}$ and $E_{j,max}$, respectively. Table 9 summarizes the group-wise values for spectrum-averaged neutron energy flux, averaged monitor cross sections as well as their uncertainties and correlation coefficients, where $j = 1-3$,

Table 9 For each neutron energy group, spectrum-averaged neutron monitor cross sections (σ_j) with fractional uncertainties and correlation coefficients derived from the IRDFF-1.05 library and fractional neutron flux calculated from the EPEN code

i	j	$E_{j,min}$ (MeV)	$E_{j,max}$ (MeV)	σ_j (b)	$\Delta\sigma_j$ (%)	$\phi_{i,j}/\sum\phi_{i,j}$	Correlation coefficient Cor(σ_j,σ_l)								
							0.246	0.600	0.800	1.000	1.200	1.400	2.200	2.400	2.600
1	1	0.246	0.600	0.0020	4.243	0.511	1.0000								
	2	0.600	0.800	0.0176	3.294	0.394	0.5098	1.0000							
	3	0.800	1.000	0.0468	3.089	0.094	0.2500	0.6346	1.0000						
2	4	1.000	1.200	0.0869	3.065	0.346	0.2594	0.2797	0.7147	1.0000					
	5	1.200	1.400	0.1290	3.019	0.489	0.2870	0.2168	0.3372	0.8172	1.0000				
	6	1.400	1.600	0.1703	2.934	0.165	0.2581	0.2960	0.2232	0.4843	0.8277	1.0000			
3	7	2.200	2.400	0.3259	2.643	0.137	0.2521	0.2370	0.2575	0.3403	0.2713	0.1734	1.0000		
	8	2.400	2.600	0.3406	2.607	0.641	0.2548	0.2657	0.2358	0.3361	0.3479	0.2576	0.8707	1.0000	
	9	2.600	2.800	0.3448	2.587	0.222	0.2283	0.2995	0.2674	0.2682	0.3314	0.3677	0.5712	0.8720	1.0000

4−6, and 7−9 groups are defined for neutron energy ($< E_n >$) = 0.60, 1.26, and 2.51 MeV, respectively.

Using the covariance matrix given in the IRDFF-1.05 library, we have propagated the covariance matrix for the present spectrum-averaged neutron monitor cross sections by using the equation 45 as given by [7]

$$Cov(< \sigma_m >_i, < \sigma_m >_k) = \sum_{j=1}^{N} \sum_{l=1}^{N} \phi_{i,j} \times \left[Cov(\sigma_j, \sigma_l) \right] \times \phi_{k,l} \qquad (10)$$

where the number of points in a given group is denoted by the letter N.

$$Cov(\sigma_j, \sigma_l) = \triangle \sigma_j \times \triangle \sigma_l \times \left[Cor(\sigma_j, \sigma_l) \right] \qquad (11)$$

After calculating the covariance matrix from the above equation, we have generated the correlation coefficients between the neutron monitor cross sections by using equation

$$Cor(< \sigma_m >_i, < \sigma_m >_k) = \left[\frac{Cov(< \sigma_m >_i, < \sigma_m >_k)}{\triangle < \sigma_m >_i \ \times \ \triangle < \sigma_m >_k} \right] \qquad (12)$$

In the literature [25,34,39], the same above process has been applied. Table 10 indicates the obtained monitor cross sections $< \sigma_m >$ for each averaged neutron energy along with its uncertainties and the correlation coefficients, which are used in further data analysis for constructing the correlation matrix between the different neutron energy ^{127}I(n,γ)^{128}I reaction cross sections.

The neutron flux calculated from the γ-ray activity of ^{115}In^m is 5.406×10^6 (14.38) n/cm^2/s at 0.60 MeV, 2.202×10^6 (7.15) n/cm^2/s at 1.26 MeV, and 3.456×10^6 (4.65) n/cm^2/s at 2.51 MeV neutron energy. In the data analysis of the neutron flux calculation, both correction factors (C$_\gamma$ and N$_{low}$) are taken in account.

The essential attributes involved in the cross section determination are the number of target atoms ($N_{s,m}$), isotopic abundance ($a_{s,m}$), γ-ray activity ($A_{s,m}$), γ-ray intensity ($I_{s,m}$), timing factor ($f_{s,m}$), detector efficiency ratio (η), and spectrum-averaged monitor cross section ($< \sigma_m >$). The total uncertainty of the measured cross section was obtained by considering the fractional uncertainty (%) from all these above attributes. However, the fractional uncertainty for the isotopic abundance (a_s) of the ^{127}I has been omitted in the present case as this element is mono-isotopic with 100% isotopic abundance. Since the present cross section measurement is the relative measurement, therefore, we have introduced the ($\eta = \varepsilon_m/\varepsilon_s$), i.e. detection efficiency ratio in the activation cross section formula as given in Eq. 4. The η value and its fractional uncertainty were propagated using the equation 39 of Ref. [7]

$$(\triangle \eta/\eta)^2 = \left[(\triangle \varepsilon_s/\varepsilon_s)^2 + (\triangle \varepsilon_m/\varepsilon_m)^2 - 2Cov(\varepsilon_m, \varepsilon_s)/(\varepsilon_s * \varepsilon_m) \right] \qquad (13)$$

where the obtained detector efficiency ratio (η) with its uncertainty is = 1.2991 ± 0.0111, and its fractional uncertainty is given in Table 11. The fractional uncertainty for the timing factor ($f_{s,m}$) was determined by the methodology given in Sec 4.1.3 of Ref. [7]. Table 11 summarizes the fractional uncertainties from the various attributes contributing to ^{127}I(n,γ)^{128}I reaction cross section. The correlation coefficient (x_1,x_2) defines the correlation between the specific associated parameter uncertainty of two energies points x_1 and x_2 MeV, and it is zero for uncorrelated (Cor(x_1,x_2) = 0) and 1 for fully correlated (Cor(x_1,x_2) = 1) [7–9]. From the obtained fractional uncertainties and correlation coefficients given in Table 11, we have calculated the total uncertainty and correlation matrix between the different energies cross sections by following Sect. 4.1.4 of Ref. [7].

Table 10 Neutron monitor cross sections for averaged neutron energy along with fractional uncertainties and correlation coefficients

Reaction	$< E_n > $ (MeV)	Cross section $< \sigma_m >$ (b)	$\Delta < \sigma_m > $ (%)	Cor($< \sigma_m >_i$; $< \sigma_m >_k$)		
^{115}In$(n, inl)^{115}$In^m	0.60	0.01266 ± 0.00042	3.3183	1.0000		
	1.26	0.12125 ± 0.00365	3.0084	0.3177	1.0000	
	2.51	0.33990 ± 0.00882	2.5950	0.2909	0.3221	1.0000

Table 11 Fractional uncertainties (%) of different attributes for all the three neutron energies and the correlation coefficient (x_1, x_2)

Attributes	Fractional uncertainties (%)			Correlation coefficient (x_1, x_2)		
	$< E_n >$=0.60 MeV	$< E_n >$=1.26 MeV	$< E_n >$=2.51 MeV	Cor(0.60, 1.26)	Cor(0.60, 2.51)	Cor(1.26, 2.51)
A_s	4.3862	6.5217	4.6607	0	0	0
A_m	13.871	6.2140	3.3729	0	0	0
I_s	0.6344	0.6344	0.6344	1	1	1
I_m	0.2178	0.2178	0.2178	1	1	1
N_s	0.0237	0.0267	0.0247	0	0	0
N_m	0.0539	0.0563	0.0522	0	0	0
a_m	0.0522	0.0522	0.0522	1	1	1
η	0.8557	0.8557	0.8557	1	1	1
f_s	0.0727	0.0753	0.0783	1	1	1
f_m	0.0106	0.0003	0.0037	1	1	1
σ_m	3.3183	3.0084	2.5950	0.3177	0.2909	0.3221
Total error (%)	14.96	9.55	6.40	0.1395	0.1285	0.2014

Table 12 Experimentally measured neutron spectrum-averaged (n,γ) reaction cross sections (in barns) for iodine with their total uncertainty and their correlation matrix

Reaction	Neutron energy $< E_n >$ (MeV)	Cross section $< \sigma_s >$	$\triangle < \sigma_s >$ (%)	Correlation matrix (x_1, x_2)		
$^{127}I(n,\gamma)^{128}I$	0.60	0.04758 ± 0.00712	14.96	1.0000		
	1.26	0.03158 ± 0.00302	9.55	0.1395	1.0000	
	2.51	0.02734 ± 0.00175	6.40	0.1285	0.2014	1.0000

3 Nuclear model calculations

The nuclear model calculations for (n,γ) reaction cross section of ^{127}I iodine nucleus have been done by using the standard nuclear reaction model codes TALYS-1.9 and EMPIRE-3.2 in the neutron energy range 0.2 to 6.0 MeV [40,41]. These codes consider the impacts of level density parameters and different reaction mechanisms, i.e. direct reaction, preequilibrium emission, and compound nucleus in estimating the cross section as a function of the incident particle energy [42–44]. We have done the theoretical calculations with the different sets of input parameters defined for different nuclear models used in the codes. The obtained theoretical results were also compared with the ENDF/B-VIII.0, JEFF-3.1/A, TENDL-2019, and JENDL-4.0 evaluated nuclear data.

In TALYS-1.9 code, the calculation was done with the predefined local optical model (OM) potential parameters described by Koning and Delaroche [45]. The Hauser–Feshbach (HFB) statistical model was used for the calculation of the compound nucleus contribution along with the Moldauer model for width correction [46,47]. The γ-ray strength function given by Brink–Axel Lorentzian formalism was used for calculating the γ-ray transmission coefficients (strength 2). For calculating the nuclear-level density parameters different models are available in the TALYS code; however, the best-estimated cross section result was obtained by using the generalized superfluid model (ldmodel 3). The important input parameters required to nuclear models for cross sections calculations were taken from the RIPL-3 library [48].

In the case of EMPIRE-3.2 code, the calculation of the nuclear level density parameters is done with the EMPIRE-specific level densities model (LEVDEN 0), which is the default model used in EMPIRE code. The optical model (OM) potentials and transmission coefficient calculations were done with the ECIS-06 code used in EMPIRE. In the ECIS-06 code calculations, the OM potential parameters described by Koning and Delaroche [45,48] were employed. The compound nucleus (CN) contribution [49] was predicted using the statistical HFB model. In addition, the HRTW model [50] was used for width fluctuation adjustments, with the default value of 3.0 MeV for the incident neutron in the EMPIRE code. In EMPIRE code, different γ-ray strength functions are available for the calculation of γ-ray transmission coefficients; however, the best-estimated cross section result was obtained by using the EGLO-enhanced generalized Lorentzian (GSTRFN 4) function.

4 Results and discussion

The experimentally measured neutron activation cross sections of (n,γ) reaction for iodine nucleus at the neutron spectrum average energy range 0.60−−2.51 MeV with its uncertain-

Fig. 6 Experimentally measured cross sections result of $^{127}I(n,\gamma)^{128}I$ reaction and its comparison with the previously measured data, theoretically predicted results, and evaluated nuclear data
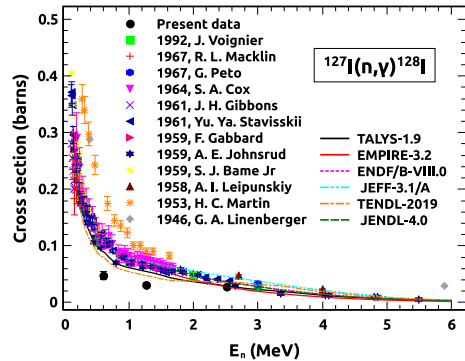
ties and the correlation matrix are summarized in Table 12, and the same is presented in Fig. 6. Other than the experimental data, we have also plotted the existing cross section data retrieved from the EXFOR database, theoretically predicted results and ENDF/B-VIII.0, JEFF-3.1/A, TENDL-2019, and JENDL-4.0 evaluated nuclear data for the detailed comparison. The present experimental cross section is represented by black colour in ellipse shape, while the various other symbols, as shown in Fig. 6, are representing the literature data from the EXFOR database. The theoretically predicted results of TALYS-1.9 and EMPIRE-3.2 are represented by black and red colour solid lines, respectively, and JEFF-3.1/A, ENDF/B-VIII.0, TENDL-2019, and JENDL-4.0 evaluated nuclear data are represented by dash-dot-dot-dash (cyan colour), dot-dot (magenta colour), dash-dot-dash (orange colour), and dash-dash (olive colour) lines, respectively. From Fig. 6, it can be observed that the present experimental results follow the existing cross section data trend, i.e. decreasing of capture cross section with increasing neutron energy. The cross sections data at energies below 2.0 MeV reported by Martin et al. [51] superseded all other existing data reported by different groups, and the present experimental results at neutron energies 0.60 and 1.26 MeV underestimate the existing and evaluated data. The cross section at 2.51 MeV, on the other hand, shows a similar trend to that seen in the cross section data reported by Johnsrud *et al.*, [52], but is lower than the cross sections reported by Stavisskii et al. [53] and Leipunskiy et al. [54], and is consistent with the evaluated nuclear data. At energy above 2.0 MeV, the TALYS-1.9 and EMPIRE-3.2 calculated cross section results are also consistent with the present measured cross section, and also the trend of excitation function results of TALYS-1.9 and EMPIRE-3.2 are consistent with the literature cross sections and ENDF/B-VIII.0, JEFF-3.1/A, TENDL-2019, and JENDL-4.0 evaluated nuclear data in the described energy range.

5 Conclusions

The neutron activation cross section for the (n,γ) reaction for the iodine nucleus has been experimentally measured in the spectrum average neutron energy range of 0.60 − −2.51 MeV in the present manuscript. The γ-ray spectra of the residue product were measured offline with the lead-shielded HPGe detector system. The quasi-monoenergetic neutrons were produced through the $^7Li(p,n)^7Be$ reaction using the charged-particle accelerator at BARC, Mumbai. $^{115}In(n,inl)^{115}In^m$ reaction was considered as a standard monitor reaction. The needful corrections resulting from the γ-ray self-attenuation process, γ-ray true coincidence summing and the low energy background neutron contribution were taken into account in the present

data analysis of the measured cross sections. The covariance analysis was performed to quantify the uncertainties of the measured cross sections and to generate the correlation matrix, which has been done very first time for the $^{127}I(n,\gamma)^{128}I$ reaction. The present experimental results follow the trend of the existing cross section curve; however, the magnitude of the cross sections obtained at energies below 2.0 MeV are lower than the existing data and the evaluated data, whereas the cross section magnitude at energy above 2.0 MeV agree well with the literature cross section data and theoretically predicted results from the codes TALYS-1.9 and EMPIRE-3.2 as well as with ENDF/B-VIII.0, JEFF-3.1/A, TENDL-2019, and JENDL-4.0 evaluated nuclear data.

References

1. V.H. Tan, P.N. Son, J. Phys. Conf. Ser. **726**, 012004 (2016)
2. S.E. Agbemava et al., Ann. Nucl. Energy **38**, 1616 (2011)
3. S.J. Bame Jr., R.L. Cubitt, Phys. Rev. **113**, 256 (1959)
4. L.A. Bernstein et al., Annu. Rev. Nucl. Particle Sci. **69**, 109 (2019)
5. National Research Council, *Distribution and Administration of Potassium Iodide in the Event of a Nuclear Incident* (National Academies Press, Cambridge, 2004)
6. Live Chart, NNDC https://www-nds.iaea.org/relnsd/vcharthtml/VChartHTML.html
7. N. Otuka et al., Radiat. Phys. Chem. **140**, 502 (2017)
8. W. Mannhurt, Report INDC(NDS)-0588 (Rev.). IAEA (2013)
9. D.L. Smith, Nuclear instruments and methods in physics research section A: accelerators. Spectr. Detect. Assoc. Equip. **257**, 365 (1987)
10. D. Neudecker et al., No. LA-UR-20-22535. Los Alamos National Lab. (LANL), Los Alamos, NM (United States, 2020)
11. N. Otuka et al., Nuclear Data Sheets **120**, 272 (2014)
12. IAEA-EXFOR Experimental nuclear reaction database, https://www-nds.iaea.org/exfor (Data retrieved on July 2020)
13. D.A. Brown et al., Nuclear Data Sheets **148**, 1 (2018)
14. R. A. Forrest, J. Kopecky, and J. C. Sublet, "The European activation file: EAF-2005 cross section library," EURATOM/UKAEA Fusion Association (2005)
15. A.J. Koning, D. Rochman, Nuclear Data Sheets **113**, 2841 (2012)
16. K. Shibata et al., J. Nuclear Sci. Technol. **48**, 1 (2011)
17. C.H. Poppe et al., Phys. Rev. C **14**, 438 (1976)
18. H. Liskien, A. Paulsen, Atomic Data Nuclear Data Tables **15**, 57 (1975)
19. P. Singh et al., Pramana **59**, 739 (2002)
20. E.M. Zsolnay, R. Capote, H.K. Nothenius, A. Trkov, *Report INDC(NDS)-0616* (IAEA, 2012)
21. R. Pachuau et al., Nuclear Sci. Eng. **187**, 70 (2017)
22. R. Pachuau et al., EPJ Web of Conferences **146** (EDP Sciences, 2017)
23. J.W. Meadows, D.L. Smith, Argone National. Laboratory (1972)
24. A.K. Bakshi et al., Nuclear instruments and methods in physics research section A: accelerators. Spectr. Detect. Assoc. Equip. **949**, 162926 (2020)
25. L.R.M. Punte et al., Phys. Rev. C **95**, 024619 (2017)
26. B. Lalremruata et al., *Report INDC(IND)-0049* (IAEA, 2017)
27. Z. Elekes, J. Timar, Nuclear Data Sheets **129**, 191 (2015)
28. J. Blachot, Nuclear Data Sheets **113**, 2391 (2012)
29. M.J. Martin, Nuclear Data Sheets **114**, 1497 (2013)
30. T. Vidmar, Nuclear instruments and methods in physics research section A: accelerators. Spectr. Detect. Assoc. Equip. **550**, 603 (2005)
31. T. Vidmar, G. Kanisch, G. Vidmar, Appl. Radiat. Isotopes **69**, 908 (2011)

32. R. Pachuau et al., Nuclear Phys. A **992**, 1216013 (2019)
33. A. Gandhi et al., Phys. Rev. C **102**, 014603 (2020)
34. A. Gandhi et al., Eur. Phys. J. A **57**, 1 (2021)
35. D.W. Millsap, S. Landsberger, Appl. Radiat. Isotopes **97**, 21 (2015)
36. E. Robu, C. Giovani, Romanian Rep. Phys. **61**, 295 (2009)
37. K. R. Jackman, "KMESS: an open source software package using a semi-empirical mesh-grid method for the modeling of germanium detector efficiencies," Dissertation (2007)
38. R. Nowotny, XMuDat: photon attenuation data on PC. IAEA Report IAEA-NDS **195**(1998)
39. S. Badwar et al., Eur. Phys. J. A **54**, 168 (2018)
40. A.J. Koning, D. Rochman, Nuclear Data Sheets **113**, 2841 (2012)
41. M. Herman, EMPIRE-3.2 Malta–Modular system for nuclear reaction calculations and nuclear data evaluation, report INDC (NDS)-0603 (p. 56). BNL-101378-2013
42. A. Gandhi et al., J. Radioanal. Nuclear Chem. **322**, 89 (2019)
43. S. Parashari, S. Mukherjee, S.V. Suryanarayana, B.K. Nayak, N.L. Rajnikant Makwana, Singh, and H. Naik, , Phys. Rev. C **99**, 044602 (2019)
44. A. Gandhi et al., Indian J. Phys. **93**, 1345 (2019)
45. A.J. Koning, J.P. Delaroche, Nuclear Phys. A **713**, 231 (2003)
46. P.A. Moldauer, Phys. Rev. C **14**, 764 (1976)
47. P.A. Moldauer, Nuclear Phys. A **344**, 185 (1980)
48. R. Capote et al., Nuclear Data Sheets **110**, 3107 (2009)
49. W. Hauser, H. Feshbach, Phys. Rev. **87**, 366 (1952)
50. H.M. Hofmann et al., Ann. Phys. **90**, 403 (1975)
51. H.C. Martin, R.F. Tascheck, Phys. Rev. **89**, 1302 (1953)
52. A.E. Johnsrud, M.G. Silbert, H.H. Barschall, Phys. Rev. **116**, 927 (1959)
53. Y. V Stavisskii, V. A. Tolstikov, and V. N. Kononov, Soviet J. Atomic Energy **10**, (1961) 153
54. A. I. Leipunskiy *et al.*, *Proceedings of Second UN Conf. on the Peaceful Uses of Atomic Energy, Geneva*, v. **15**, 1–13 September 1958, p. 50-59 (P/2219)